Taylor & Francis
Taylor & Francis Group

Canadian Journal of Remote Sensing
Journal canadien de télédétection

ISSN: 0703-8992 (Print) 1712-7971 (Online) Journal homepage: http://www.tandfonline.com/loi/ujrs20

Processing Methodology Based on ASTER Data for Mapping Mine Waste Dumps in a Semiarid Polysulphide Mine District

Alejandro Rodríguez-Hernández, Roberto Briones-Gallardo, Israel Razo, Cristina Noyola-Medrano & Isabel Lázaro

To cite this article: Alejandro Rodríguez-Hernández, Roberto Briones-Gallardo, Israel Razo, Cristina Noyola-Medrano & Isabel Lázaro (2016): Processing Methodology Based on ASTER Data for Mapping Mine Waste Dumps in a Semiarid Polysulphide Mine District, Canadian Journal of Remote Sensing, DOI: 10.1080/07038992.2016.1197037

To link to this article: http://dx.doi.org/10.1080/07038992.2016.1197037

Accepted author version posted online: 03 Jun 2016.
Published online: 03 Jun 2016.

Processing Methodology Based on ASTER Data for Mapping Mine Waste Dumps in a Semiarid Polysulphide Mine District

Alejandro Rodríguez-Hernández[1], Roberto Briones-Gallardo[*,1], Israel Razo[2], Cristina Noyola-Medrano[2], Isabel Lázaro[1]

[1]Facultad de Ingeniería - Instituto de Metalurgia, Universidad Autónoma de San Luis Potosí, Sierra Leona No. 550, Col. Lomas 2a Secc., 78210 San Luis Potosí, S.L.P., México

[2]Facultad de Ingeniería, Universidad Autónoma de San Luis Potosí, Av. Manuel Nava #8. Zona Universitaria 78290, San Luis Potosí, S.L.P. México

Received 18 December 2015. Accepted 27 May 2016.

[*]Corresponding author e-mail: briones@uaslp.mx

Abstract

The aim of this work is to present a simple, economic and efficient methodology based on the use of ASTER data to map areas of mining waste composed of heterogeneous mineral mixtures. This methodology has been applied to the District of Santa María de la Paz, Mexico, to detect different mineral phases that have been previously characterized. The methodology consists of techniques such as band ratioing, Normalized Difference Tailings Index (NDTI) and Spectral Angle Mapper (SAM) classification. Experimentation with the SAM classification has established a minimum threshold of 0.08 radians for the mapping of mining waste and tailings impoundments. The results of this analysis indicate that the different techniques applied to ASTER images do not show the same level of accuracy for all waste dumps. In this study, the best technique for mapping the different mine wastes is the ferrous iron ratio, which features an overall

accuracy of 93.25% and a kappa coefficient of 0.86. The accuracy of the results suggest that the proposed methodology can be used in the detection of mine waste in mining districts that have not been fully characterized, especially in countries with a large amount of abandoned mining waste.

Résumé

Le but de ce travail est de présenter une méthodologie simple, économique et efficace, basée sur l'utilisation des données ASTER pour cartographier les zones de résidus de mine. Cette méthodologie appliquée dans le secteur minier de Santa Maria de la Paz au Mexique, détecte différentes phases minérales qui ont été largement caractérisées dans le passé. La méthodologie consiste en des techniques telles que le rationnement de bande, l'Indice de Différence Normalisé des Résidus (NDTI) et la classification par la méthode Spectral Angle Mapper (SAM). L'expérimentation avec la classification de SAM permet d'établir que le seuil minimal exigé pour cartographier les déchets minière et les bassins de résidus est 0.08 radians. Les résultats de cette analyse indiquent que les différentes techniques appliquées aux images ASTER ne montrent pas le même niveau d'exactitude pour tous les résidus de mine. Dans cette étude, on a observé que la meilleure technique pour cartographier les différents déchets miniers est l'indice d'oxyde ferreux. Pour cette dernière technique, la précision globale est de 93,25% et le coefficient kappa est 0,86. L'exactitude des résultats suggère que la méthodologie proposée peut être utilisée dans la détection des résidus miniers pour les districts miniers qui ne sont pas entièrement caractérisés, notamment dans des pays avec une grande quantité de déchets miniers abandonnés.

1. Introduction

For many centuries, mining and metallurgical activities, such as exploration, mining, mineral processing and extractive metallurgy, have produced diverse environmental impacts, including the production of solid wastes that have resulted in waste rock, tailings and slag. The issues associated with abandoned mines include physical, environmental and public safety hazards, posed principally by the physical and chemical stability of the mine waste dumps. While it is impossible to estimate the number of former mining sites that exist around the world, Van Zyl et al. (2002) presented a compilation of the available data on approximately 622,371 abandoned mine sites registered in different countries, such as Australia, Canada, the United Kingdom, the United States, South Africa, Ireland, Sweden, Japan and Chile. However, these countries are not a complete list of all the existing sites in the world, and the magnitude of the environmental impacts in countries with a long mining history is often considerable.

In Mexico, the database of the National Institute of Geography and Statistics (INEGI, 2014) has a record of 4,464 mining sites, but information on the environmental impacts of these sites is currently lacking. The intense exploitation of epithermal deposits in this country has altered the local surface, covering the ground and vegetation with mining waste. Because waste dumps are not covered, they are susceptible to erosion by wind and water (Ramos-Arroyo et al., 2004). For example, in the mining district of Guanajuato, which is the most representative in Mexico, there is an estimated record of approximately thirty-two cyanidation and bulk-flotation tailings dumps covering an area of 82.5 hectares and featuring an estimated weight of 40.3 million tons. Additionally, an estimated 20 million tons of amalgamation tailings are present in river sediments in Guanajuato (Ramos-Arroyo et al,. 2004; Ramos-Arroyo and Siebe-Grabach, 2006).

Identifying and assessing the impacts of historical mining activities is a complex process, and even though the mining sites share similar regional geological conditions, they can differ in terms of certain characteristics, such as the mineralogy of the deposits, local geology, climate, hydrology, topography, type of mining, processing and metallurgical processes of each mine. Furthermore, there is a lack of interest and investment in the evaluation of abandoned mine sites, especially in developing countries. Additionally, in these areas, most advanced applications of remote sensing technologies and sensors focus on geological applications using expensive resources, not always affordable by developing countries. Hence, it is necessary to develop and apply new remote sensing methodologies that permit the location and identification of mineral pollutant sources in abandoned mine sites in an efficient, economical and straightforward manner as a part of environmental impact assessment studies.

Remote sensing can be used for environmental monitoring of mining and metallurgy activities because of the characteristics of certain environmental variables, such as the presence of primary and secondary minerals deposited anthropically on the surface of the mining sites. The detection of minerals on the surface of the Earth using remote sensing is based on specific interactions between the minerals and electromagnetic radiation, specifically in the wavelength range of 0.4 μm to 14 μm (Cudahy et al., 2008). Hyperspectral sensors, such as the Airborne Visible/Infrared Imaging Spectrometer (AVIRIS), commonly collect more than 200 spectral bands and exhibit a better ability to discriminate among specific minerals because of its high spectral resolution. However, these sensors feature a greater level of complexity and a higher cost of scene acquisition, and some areas lack scenes or coverage. In contrast, multispectral sensors have a limited number of spectral bands, but some systems, such as Landsat 8 and

ASTER (Advanced Spaceborne Thermal Emission and Reflection Radiometer), provide world coverage at a moderate temporal resolution, which makes them suitable for geological and environmental applications. The structure of ASTER images is shown in Table 1. The VNIR subsystem of ASTER is especially useful for topographic interpretation and can assess vegetation and iron oxide minerals in surface soils and rocks (Yamaguchi et al., 1999). Similarly, the SWIR has been shown to be able to make compositional determinations and mineral maps by measuring spectral absorption features related to molecular structures in carbonate, hydrates, hydroxyl-bearing sulfate, silicate and other minerals (Mars and Rowan, 2010). Therefore, the characteristics of the ASTER system and its relatively low cost make it suitable for identifying and mapping surface disturbances related to mining-related pollution.

To date, the ASTER system has primarily been used to detect superficial changes in different land cover types (vegetation, urban zones, and mining areas) over time (Charou et al., 2010). Nevertheless, some previous studies have used ASTER data to map mine waste zones in mineral districts. In this way, Schimmer (2008) identified the location of active copper tailings using the Normalized Difference Tailings Index (NDTI). Chevrel et al. (2005) mapped the distribution of iron oxides and silicate minerals. Mezned et al. (2008) showed the usefulness of spectral libraries to identify the presence of certain minerals, such as quartz, calcite, kaolinite, galena, cerussite, pyrite, sphalerite, hematite, goethite, gypsum, barite and fluorite, which are difficult to identify in the mining waste.

Therefore, this study aims to identify and map the mine waste dumps in the study area that have already been reported as important sources of pollution in order to evaluate and test the

usefulness of ASTER images and the methods proposed. The study area was selected because there is enough information to validate the results obtained from the different techniques applied to the ASTER images and this area is representative of the current status of the north-central mining district zones of Mexico, where polysulfide metallic minerals have been exploited intensively since colonial times (Chavez et al., 1999; Razo et al., 2004).

2. Study Area

The mining district of Santa Maria de la Paz is located in northern San Luis Potosi State, Mexico. Its area of influence is within the towns of Villa de la Paz and Matehuala and is bounded by the eastern hillsides of a small mountain known as “El Fraile” (Figure 1), located in the Sierra Madre Oriental mountain range and featuring an elevation of approximately 2,000 m above sea level (Gunnesch et al., 1994). The climate of the Villa de la Paz zone is dry and semiarid, with cool winter and summer rain. A very similar climate is observed in the town of Matehuala but with warmer summers and an average annual precipitation of approximately 470 mm (SGM, 2008). Figure 2 shows the different climograms for two meteorological stations, corresponding to the closest locations to Villa de la Paz and Matehuala. The graphics show the relationship between altitudinal gradient and the climate. Then the highest temperatures are in the northern valley of Matehuala where weathering processes are generating areas of high salinity, due to the high rate of evapotranspiration.

Two polysulfide ore deposits had been discovered by the end of the 18th century and have been intensively exploited for more than 200 years in this site. These deposits are hosted in Upper Cretaceous limestone-dominant strata (Gunnesch et al., 1994) (Figure 3). The first deposit

consists of Cu-Au skarn mineralization, and the second consists of hydrothermal Ag-Pb-Zn veins. The primary minerals associated with the mineralization of the Cu-Au skarn are chalcopyrite ($CuFeS_2$), bornite (Cu_5FeS_4), sphalerite (ZnS), pyrite (FeS_2) and arsenopyrite (FeAsS) (Megaw, 1999). The Ag-Pb-Zn mineralization comprises a series of hydrothermal veins with the presence of sulfides such as galena (PbS), sphalerite (ZnS), arsenopyrite (FeAsS), pyrite (FeS_2) and Cu-Sb sulfosalts (SGM, 2008). The N-S-striking Dolores fault separates the western Cu-Au skarn from the eastern hydrothermal Ag-Pb-Zn vein system (Pinto-Linares et al., 2008). In this region, Chiprés et al. (2009) found that the regional background concentrations of arsenic in the A horizon of soils in non-impacted or non-mineralized areas ranges from 4 to 35 mg/kg and that the local background associated with diffuse mineralization and fluvial dispersion of eroded material from areas of higher As concentrations ranges from 35 to 80 mg/kg. Finally, Razo et al. (2004) found that the highest As concentrations associated with strong environmental impacts produced by the dispersion of material from mine waste reached maximum values of 11,930, 17,384 and 28,599 mg/kg As in urban areas, rural areas and dry sediment impacted by acid mine drainage, respectively. The primary gangue minerals aside from the ferrous silicates produced by hydrothermal alteration found in this site are quartz (SiO_2), calcite ($CaCO_3$), and pyrite (FeS_2) (Levresse et al., 2012).

The soils adjacent to Villa de la Paz are classified as calcic to gypsic xerosols, whose mineralogy is composed mainly of calcite and gypsum and the amount of quartz and clay minerals is generally bellow 5% (Castro-Larragoitia et al., 1997). As a result of the mining and metallurgy activities in this region, solid waste has been generated, but its disposal has been inadequate. The sources of these solid wastes have been visually and bibliographically identified

(Figure 3) as (a) from mining waste, deposited as waste rock in the hillsides of "El Fraile" and within Villa de la Paz (W1, W2, W3, W4, W5, H1, H2); (b) from mineral processing waste, deposited as tailings impoundments within the limits of Villa de la Paz (T1, T2, T3, T4); and (c) from metallurgy operations, deposited as slag dumps north of the urban zone of Matehuala (SL) (Manz and Castro, 1997; Razo et al., 2004).

The tailings and waste rock dumps located in Villa de la Paz are physically unstable due to the slope of the impoundment, which makes it susceptible to erosion by both water and wind. Likewise, the dumps are chemically unstable, as they contain polymetallic sulfide mineral phases that can suffer oxidation reactions (Razo et al., 2004). Given that these dumps have not been covered, the wind- and water-driven dispersion of dust material cannot be prevented. Strong winds have been demonstrated to disperse material from the tailing impoundments, as these winds blow from the south to the north from May to August and from the northeast to the southeast from November to February (Razo et al., 2004). Furthermore, there is evidence of hydric erosion during the rainy season, when the drainage system carries material from the waste dumps located in Villa de la Paz on the western hillsides of "El Fraile" towards the northeastern Matehuala valley. These processes have contaminated an area of approximately 100 km^2 surrounding the town of Villa de la Paz, producing a halo of high concentrations of As, Pb, Cd, Zn and Cu that are above national and international guidelines for soils (Castro-Larragoitia et al., 1997; Razo et al., 2004; Espinosa-Reyes et al., 2014), surficial water and groundwater (Martínez-Villegas et al., 2013). In the other hand, the pollution of the soils in the northern of Matehuala appears to be caused by smelter emissions and historical residues with high concentrations of Pb, As and Cd (Manz and Castro, 1997). Additionally Yáñez et al. (2003) have shown that the high

levels of arsenic and lead have increased the frequency of genotoxicity in children in the urban zone of Villa de la Paz, where ingestion of contaminated household dust and soil are the principal pathways of exposure (Mejía et al., 1999). It is important to remember that arsenic, for example, is a well-documented human carcinogen and lead has several neurological effects in children like decrease of the intelligence quotient, cognitive functions and is related to behavior disorders. However on this site, the children population has not been epidemiologically analyzed looking for these kind of diseases.

3. ASTER Data Set

The analysis of the Santa Maria de La Paz site was based on two scenes. The acquisition dates of the selected scenes were April 30th, 2006 and February 26th, 2012. The 2006 scene was selected because it was the last available scene that included SWIR data (which was relevant for mineral detection) due to the instrument becoming inoperable in 2008. The image from 2012 corresponds to the last available scene that included VNIR data. The ASTER data obtained with the authorization of the Land Processes Distributed Active Archive Center (LP DAAC, 2014) consisted of the surface reflectance in the VNIR and SWIR wavelengths and included a crosstalk correction (AST_07XT) and data on surface emissivity in the TIR wavelengths (AST_05). These data are in line with the aims of this study, as the percentage of cloud coverage is zero over the zone of interest and the date of acquisition corresponds to the dry season, thereby minimizing the effect of green vegetation in the study area.

4. Methodology

1.1 *Pre-processing of the ASTER data*

The data were pre-processed at a pixel size of 15 m by resampling the SWIR data and integrating it with the VNIR data. The TIR wavelengths were managed separately with an original resolution of 90 m. The study area was cropped (Figure 4) from the complete ASTER scenes in order to simplify and shorten processing times. The urban areas and the green vegetation spectral values interfere with the Mg-OH band ratio operations; thus, these areas were removed applying a mask consisting of dividing the band 3 reflectance values by the band 2 values and the subsequent elimination of values greater than 1.75 (Cudahy, 2012).

1.2 *Processing of the ASTER data*

1.2.1 Spectral enhancement using band ratio transformation

Band ratioing has proven to be useful for highlighting certain features or materials that cannot be seen in the raw bands (Campbell and Wynne, 2011). Some band ratios described by Cudahy (2012) were chosen and tested in this work for the study area with the aim of detecting mineral groups that could be indicative of mine waste disposal zones (Table 2) by taking into account the mineralization of the study area and the type of mining operation present at the site. The band ratio 5/4 was chosen to detect ferrous iron (Fe^{+2})-bearing alteration minerals present in skarn mineralization and hence found in gangue materials. These minerals are discernable in the ASTER data due to a steep increase in the reflectance values of the bands 4 and 5 (Rowan et al., 2005). The band ratio 13/10 was chosen to detect quartz minerals and siliceous materials, which

are commonly present in gangue material from intrusive deposits and in the slag from smelter sites. Quartz has very prominent spectral features in the TIR region, showing absorption features in bands 10 and 12 and resulting in higher emissivity in band 13. Finally, the band ratio (6+9)/(7+8) was chosen to detect the content of Mg-OH-bearing minerals present in rocks associated with hydrothermal propylitic alteration and in gangue material from mining operations, as this ratio enhances the absorption features present in the range of bands 7 and 8 (Cudahy, 2012).

The resulting output ratios require segmentation of the results so that only the pixels with the highest probability of finding the minerals of interest appear. This process has been performed with the aim of obtaining more precise maps of the mine wastes and to reduce the amount of interference or false positive output results in the scene. The statistics for the three band ratio products were calculated, and each result was segmented using the mean value + 2.3 × the standard deviation. This specific value was then used to segment the highest 1% of the values that have the highest probability of corresponding to the target mineral groups. This segmentation method has been used by Rouskov et al. (2005) to map iron oxides and clay minerals using band ratio operations.

1.2.2 Classification using the Spectral Angle Mapper algorithm

The Spectral Angle Mapper (SAM) algorithm has been selected for the classification of mine waste in this work. The SAM algorithm is a useful tool that permits rapid and easy mapping of the spectral similarity between image spectra and reference spectra by calculating the angle between them, treating them as vectors in a space with a dimensionality equal to the number of

bands. Additionally, it is not perturbed by illumination differences due to topography in areas of low to moderate relief and high sun angles (Kruse et al., 1993). This work seeks to test the ability of the SAM algorithm to classify certain minerals in mixtures present in mine waste dumps in the study area by comparing the ASTER data with some reference spectra from the United States Geological Survey (USGS) spectral library resampled to the ASTER spectral resolution. The USGS Spectral Library was used in this study because it contains reference spectra for certain primary and secondary minerals that could be indicative of deposition zones of mine waste. Hence, the use of these data could help to map the mine waste zone by means of mineral detection. Nevertheless, the main disadvantage of the SAM algorithm is that it does not consider the sub-pixel value for different minerals. Therefore, given that mine wastes are heterogeneous mixtures of gangue, ore minerals and alteration products, their spectral mixture could become problematic, and incorrect mineral classifications could be made.

The resampled spectra used to classify the image in this study are shown in Figure 5. The hematite 3 spectrum was chosen to detect ferric iron (Fe^{+3})-bearing minerals because it was the best reference spectrum for conclusively detecting mine wastes. The orthoclase 1 spectrum was chosen because it is present in the two mineralization types at the study site (Pinto-Linares et al., 2008). The quartz 2 spectrum was chosen to detect quartz present as gangue products in the study area. In other studies, the thresholds used in SAM classifications vary widely depending on the target minerals and the characteristics of the study areas (Di Tommaso and Rubinstein, 2007; Pour and Hashim, 2012; Rajendran et al., 2013). Therefore, the threshold value in radians used in this work was adjusted by experimenting with different values to find the lowest possible value that produced selective results for the classification of mining waste and tailings impoundments.

1.2.3 Normalized Difference Tailings Index

The Normalized Difference Tailings Index is an operation that helps to identify mine wastes, such as copper mining tailings impoundments, through (a) the absence of either organic material and/or vegetation, (b) a homogeneous particle size and (c) waste wetness (Schimmer, 2008). This method is based on the application of a Normalized Difference Vegetation Index (NDVI), in which Schimmer (2008) recommends selecting a specific range of the resulting values of the index. In this work, the range was adjusted from -0.075 to 0.075 with the goal of discriminating the tailings dumps in the scene. Equation (1) was applied to evaluate the feasibility of mapping the mine wastes using the NDVI operation.

$$\mathrm{NDTI} = -0.075 < \mathrm{NDVI} < 0.075 = 0.075 < \left(R_{B3} - R_{B2} / R_{B3} + R_{B2}\right) < 0.075 \quad (1)$$

where R_{B3} is the band 3 reflectance and R_{B2} is band 2 reflectance of the ASTER system. The segmentation is converted into vectors and was exported as a shapefile that was integrated into the other layers.

1.2.4 Validation of the results

The overall accuracy and kappa coefficient (κ) of each classification output image was evaluated using confusion matrixes (Table 3), which identify not only overall errors for each category but also misclassifications. The κ determines whether the agreement between the performed classification and the reference data is significantly better than a random classification. Producer and user accuracies are ways of representing individual category accuracies. User accuracy corresponds to errors of commission (inclusion), and producer accuracy corresponds to errors of omission (exclusion). The matrix analysis shows how the

classification represents actual areas on the landscape (Congalton and Green, 2009). Each column of the confusion matrix represents a ground truth class, and the values in the column correspond to the labeling of the ground truth pixels by the image classification (Campbell and Wynne, 2011). In this study, the ancillary data, referred to as the ground truth information, correspond to the known locations of different types of mine waste dumps described in the literature on the study area and have been verified through previous field inspections. The evaluation areas for accuracy assessment were determined using this previous information (Figure 1). Because the results of each classification involved the mapping of the same areas of mining waste in the image, a confusion matrix is presented for each classification method, and the results of each classification are grouped into two classes labeled as (a) mine wastes and (b) no mine wastes. Due to the different types of mine waste present in the area (waste rock, tailings and slag) and the differences between their mineralogies, it is expected that some classification methods will not map all the types of mine wastes. In this scenario, the evaluation areas assigned in the accuracy assessment will only be those that correspond to the type of mine waste mapped, in order to show the selectivity of some classification methods for a specific type of mine waste.

5. Results and discussion

The resulting output ratios and their respective segmentations are shown in Figure 6. For the possible spread of (Fe^{2+})-bearing minerals, the band ratio 5/4 values greater than 0.879 in a population of at least 10 pixels are mapped as a red polygon layer in the second band of the ASTER scene (Figure 6a'). The geographic distribution of the mapped red areas corresponds to different types of mine wastes. The mapped waste rocks W1 and W2 are located to the northwest

and west of Villa de la Paz. Additionally, the mineral processing plant and the tailings impoundment T1 and T3 are mapped on the east side of Villa de la Paz. Finally, the slag dumps (SL) are also mapped in red to the north of Matehuala (Figure 6a'). This approach was considered because ferrous silicates are a component of the minerals present at the site and are therefore contained in the mine wastes. Likewise, the silicates that are present as gangue minerals subjected to flotation were discarded to the tailings impoundment following concentration (SGM, 2008) and were introduced as a melting reagent in the smelting process, subsequently becoming slag residues. This band ratio shows the best overall accuracy (93.3%) of all the classifications and has a κ of 0.86 (Table 3). This classification also mapped the surroundings of the tailings impoundment T1 as mine waste, which is attributed to the dispersion of material from this dump (Razo et al., 2004).

The distribution of silica/quartz minerals is mapped on Figure 5b'. The silica index (band 13/band 10) is shown over the study area as a blue polygon layer and corresponds to band ratio values greater than 1.016 grouped in populations of at least 2 pixels. The geographic distribution of the mapped blue areas corresponds first to the intrusive deposit located in "El Fraile" mountain, located on the east side of Villa de la Paz, second to the tailings impoundment T1, also located on the east side of Villa de la Paz, and finally to the slag deposit (SL) to the north of Matehuala. The yellow polygon layer over the study area in Figure 6c' highlights the presence of Mg-OH-bearing minerals. The yellow polygons correspond to band ratio values greater than 1.145 grouped in populations of at least 10 pixels and represent the slags deposit located to the north of Matehuala city. Some small isolated areas to the north of Villa de la Paz were also

identified, but the field inspection revealed that these sites corresponded to cropland surrounding the town.

The Mg-OH band ratio and the silica index both identified the zone where the slag from the old Matehuala smelter was deposited (Figures 6b' and 6c'). The Mg-OH index has an overall accuracy of 81.1% and a κ of 0.62 for the specific detection of slag (Table 3). However, as previously mentioned, the silica index also mapped part of the mineralized area in "El Fraile" mountain and the tailings impoundment T1, most likely because quartz is one of the main gangue products in this site due to the flotation process (SGM, 2008). The silica index has an overall accuracy of 91.2% and a κ of 0.82 for detecting tailings impoundments and slag deposits (Table 3).

As a result of this work, the smallest possible threshold value that allowed the mapping of mining waste and tailings impoundments in the SAM classifications was 0.08 radians. The SAM classification for the reference spectrum of USGS Hematite 3 was very useful and selective for detecting the tailings impoundment T3, as shown in the cyan polygon layer in Figure 7a. This classification has an overall accuracy of 90.2% and a κ of 0.80 for the detection of the T3 tailings dump specifically (Table 3). Based on the field observations, the T3 dump, unlike other impoundments, features a reddish, opaque surface that could be associated with crystalline phases of iron oxides.

The SAM classifications of orthoclase 1 and quartz 2 were also tested. The SAM method identified orthoclase in the tailings impoundment T1, as shown by the orange polygon layer in Figure 7b. This is expected given that this mineral is present in the mineral deposits. Likewise, it

was possible to map quartz using the SAM algorithm, as is shown in the purple polygon layer in Figure 7c. The spectra of the pixels mapped by the three different SAM classifications are shown in Figure 5 as pixels identified as a') hematite, b') orthoclase and c') quartz. The mapped pixel spectra are clearly not identical to the resampled reference spectra; however, the spectral behavior through all nine bands of the ASTER VNIR and SWIR is similar enough to make classification possible under a threshold of 0.08 radians. Markoski and Rolim (2012) showed that the application of the SAM algorithm to ASTER data can efficiently characterize mining residues. The difference between the resampled reference and mapped pixel spectra is possibly due to the high content of carbonates, hydrothermally altered products and others rocks that generally show strong spectral signatures while reducing the spectral intensity of other minerals that are present in lower concentrations. In this case, for instance, the existence of orthoclase and quartz phases was already known. The accuracy assessment for the orthoclase and quartz SAM operations shows that these classifications have an overall accuracy of 85.3% and 86.3%, respectively, and a κ of 0.70 and 0.72, respectively (Table 3).

The results of multiplying the output of the NDTI operation by -1 are shown in Figure 6d, and the final classification is shown as a green polygon layer in Figure 6d'. The mine waste can be mapped by stretching and segmenting the resulting index values within the range of -0.075 to 0.075 instead of the value range of -0.39 and -0.35 on a scale from -1 to 1 proposed by Schimmer (2008). The value range selected here helps to identify not only the flotation tailings impoundments but also the waste rocks dumps from mining operations. Additionally, Kopačková (2014) used the NDVI operation to map exposed surfaces in a mining site based on NDVI values of less than 0.4.

The ASTER scene from 2012 indicated the appearance of a new waste rock dump (W3) and an increase in the previously described W1 and W2 dumps. To differentiate and reduce interferences in the mapping of waste dumps, the Matehuala and Villa de la Paz urban zone polygons were masked. The resulting NDTI classification has an overall accuracy of 79.86% and a κ of 0.59 (Table 3). Finally, all the results were integrated to produce a final layer that showed all the detected mine waste dumps. This layer is shown in Figure 8. Notably, only three dumps (W5, H1, and H2) could not be mapped or did not show any signal, likely due to the changes experienced by these dumps over time. For example, changes in the superficial material above the W5 dump are known to have been caused by partial paving of the dump, and changes in H1 were caused by the construction of a recreational area with a "viewpoint". Furthermore, a baseball stadium was built on the location of H2. Finally, the vegetation cover that has grown on T4 has made it difficult to completely map this dump, and this has been confirmed by the field observations.

The ASTER SWIR data were particularly useful for the realization of this work, as the ferrous iron index, the Mg-OH ratio and the three SAM classifications were performed using these bands. The three bands of VNIR data were also part in the performance of the SAM classifications, made over the VNIR and SWIR data and proved to be useful also in the application of the NDTI operation in the mapping of the mine waste. Due to the low resolution of the TIR data, these data were only useful in the mapping of large tailings deposits (e.g., T1) using the silica index.

6. Conclusions

This study was able to map and locate 9 of the 12 mine waste dumps that have been documented previously and verified by field observations. Accuracy assessment showed that the band ratios and the SAM classifications present high values of overall accuracy. The band ratio 5/4 (ferrous iron) was the best method to map all the types of mine wastes, whereas some techniques applied to the ASTER data identified only certain type of wastes. However, it was not possible to detect three of the reported dumps (W5, H1 and H2) due to anthropogenic activity and the presence of vegetation cover. The application of the SAM technique with a threshold of 0.08 radians proved to be an effective method to map the possible distribution of reference minerals. This technique also provided important information related to the mineralogical composition of the mine wastes, even though the TIR region could not be compared due to the lack of these data in the USGS spectral library. The band ratios and the SAM were useful in this work for the identification of mineral phases present in the mineral gangue and mineral processing products. The band ratios proved to be better than the SAM and the NDTI methods in the mapping of mining waste because the band ratio technique resulted in a better overall accuracy assessment score and was the only technique that completely mapped the large slag deposit and tailings impoundments. In contrast, the SAM classifications produced many false positive results that represented urban zones of Matehuala and Villa de la Paz.

Each mapping technique produces very specific results for each type of waste. Therefore, integrating all the results is suggested in order to obtain a broader overview of the pollution in the region (Figure 8). Additionally, the integration of these results with other sources of information, such as topography, hydrology, climate conditions and the location of urban zones,

represents a useful method for the design of soil and waste sampling surveys during field investigations and environmental evaluations of mining sites, particularly historic ones. However, the presented methodology requires distinguishing between the interference associated with urban zones and possible mine waste locations. These areas can be separated by the application of field knowledge as well as visual interpretation of the Aster data. It is also important to understand the natural and anthropogenic processes that produced the mineral distribution on the site surface. Regardless, the use of the proposed methodology applied to ASTER data is useful in the classification of mine waste in environments with large amounts of abandoned and uncharacterized mining waste.

Acknowledgements

The ASTER data AST_07XT and AST_05 were courtesy of the online Data Pool at the NASA Land Processes Distributed Active Archive Center (LP DAAC), USGS/Earth Resources Observation and Science (EROS) Center, Sioux Falls, South Dakota (https://lpdaac.usgs.gov/data_access/data_pool). This work was financially supported by project FORDECYT grant number 190966 and CONACYT under scholarship number 297730.

References

Campbell, J.B., and Wynne, R.H. 2011. *Introduction to remote sensing*. 5th edition. Guilford Press, New York.

Castro-Larragoitia, J., Kramar, U., and Puchelt, H. 1997. 200 years of mining activities at la PAZ/San Luis Potosí/Mexico — consequences for environment and geochemical exploration. *Journal of Geochemical Exploration*, Vol. 58, No. 1, pp. 81–91. DOI: 10.1016/S0375-6742(96)00054-4.

Charou, E., Stefouli, M., Dimitrakopoulos, D., Vasiliou, E., and Mavrantza, O.D. 2010. Using remote sensing to assess impact of mining activities on Land and water resources. *Mine Water and the Environment*, Vol. 29, No. 1, pp. 45–52. DOI: 10.1007/s10230-010-0098-0.

Chavez, L., Alarcón, F., and Parga, J. 1999. Mining exploration potential of VMS and carbonate hosted Polymetallic deposits in Central Mexico. In *VMS and carbonate-hosted Polymetallic deposits of Central Mexico.* Edited by J.L. Jambor. British Columbia and Yukon Chamber of Mines, Vancouver. pp. 1–13.

Chevrel, S., Bourguignon, A., Cottard, F., and Itard, Y. 2005. Exploitation of ASTER imagery in mining-related environmental management In *Pecora 16 - global priorities in land remote sensing*. October, Sioux Falls. pp. 23-27.

Chiprés, J.A., Castro-Larragoitia, J., and Monroy, M.G. 2009. Exploratory and spatial data analysis (EDA–SDA) for determining regional background levels and anomalies of potentially toxic elements in soils from Catorce–Matehuala, Mexico. *Applied Geochemistry*, Vol. 24, No. 8, pp. 1579–1589. DOI: 10.1016/j.apgeochem.2009.04.022.

Congalton, R.G., and Green, K. 2009. *Assessing the accuracy of remotely sensed data*. CRC Press, Taylor & Francis, Boca Raton.

Cudahy, T. 2012. *Satellite ASTER geoscience product notes for Australia*. CSIRO ePublish No. EP-30-07-12-44. Available from [cited December 17, 2015].

Cudahy, T., Jones, M., Thomas, M., Laukamp, C., Caccetta, M., Hewson, R., Rodger, A., and Verrall, M. 2008. *Next generation mineral mapping: Queensland airborne HyMap and satellite ASTER surveys 2006-2008*. CSIRO Exploration and Mining, Bentley. Report P2007/364. Available from [cited December 17, 2015].

Di Tommaso, I., and Rubinstein, N. 2007. Hydrothermal alteration mapping using ASTER data in the Infiernillo porphyry deposit, Argentina. *Ore Geology Reviews*, Vol. 32, No. 1-2, pp. 275–290. DOI: 10.1016/j.oregeorev.2006.05.004.

Espinosa-Reyes, G., González-Mille D. J., Ilizaliturri-Hernández C. A., Mejía-Saavedra J., Cilia-López V. G., Costilla-Salazar R., and Díaz-Barriga F.. 2014. "Effect of Mining Activities in Biotic Communities of Villa de La Paz, San Luis Potosi, Mexico." *BioMed Research International* 2014: 13.

Gunnesch, K.A., Torres del Angel, C., Castro, C.C., and Saez, J. 1994. The Cu-(Au) Skarn and Ag-Pb-Zn vein deposits of la PAZ, Northeastern Mexico; mineralogical, paragenetic, and fluid inclusion characteristics. *Economic Geology*, Vol. 89, No. 7, pp. 1640–1650. DOI: 10.2113/gsecongeo.89.7.1640.

INEGI (Instituto Nacional de Estadistica y Geografia). 2014. *Geología, Datos vectoriales escala 1:1000000 descarga*. Available from [cited December 17, 2015].

Kopačková, V. 2014. Using multiple spectral feature analysis for quantitative pH mapping in a mining environment. *International Journal of Applied Earth Observation and Geoinformation*, Vol. 28, pp. 28–42. DOI: 10.1016/j.jag.2013.10.008.

Kruse, F.A., Lefkoff, A.B., Boardman, J.W., Heidebrecht, K.B., Shapiro, A.T., Barloon, P.J., and Goetz, A.F.H. 1993. The spectral image processing system (SIPS)—interactive visualization and analysis of imaging spectrometer data. *Remote Sensing of Environment*, Vol. 44, No. 2-3, pp. 145–163. DOI: 10.1016/0034-4257(93)90013-N.

Land Processes Distributed Active Archive Center (LP DAAC). 2014. *ASTER level 2 surface reflectance and level 2 surface emissivity*. Version 3. NASA EOSDIS Land Processes DAAC, USGS Earth Resources Observation and Science (EROS) Center, Sioux Falls, South Dakota. Available from <https://lpdaac.usgs.gov> [cited March 7, 2014]. DOI: 10.5067/ASTER/AST_07XT.003 and 10.5067/ASTER/AST_05.003.

Levresse, G., Pinto-Linares, J., and Tritlla, J. 2012. Gold copper skarn fluid evolution in the La Paz Deposit, San Luis Potosi, Mexico. In *GEOFLUIDS VII – International Conference IFP Energies Nouvelles*. Rueil-Malmaison, France. June 6-8.

Manz, M., and Castro, L.J. 1997. The environmental hazard caused by smelter slags from the Sta. Maria de la PAZ Mining District in Mexico. *Environmental Pollution (Barking, Essex: 1987)*, Vol. 98, No. 1, pp. 7–13. DOI: 10.1016/S0269-7491(97)00107-3.

Markoski, P.R., and Rolim, S.B.A. 2012. Evaluation of aster images for characterization and mapping of amethyst mining residues. *ISPRS Annals of Photogrammetry, Remote Sensing and Spatial Information Sciences*, Vol. I-7, pp. 153–58. DOI: 10.5194/isprsannals-I-7-153-2012.

Mars, J.C., and Rowan, L.C. 2010. Spectral assessment of new ASTER SWIR surface reflectance data products for spectroscopic mapping of rocks and minerals. *Remote Sensing of Environment*, Vol. 114, No. 9, pp. 2011–2025. DOI: 10.1016/j.rse.2010.04.008.

Martínez-Villegas, N., Briones-Gallardo R., Ramos-Leal J. A., Avalos-Borja M., Castañón-Sandoval A. D., Razo-Flores E., and Villalobos M.. 2013. "Arsenic Mobility Controlled by Solid Calcium Arsenates: A Case Study in Mexico Showcasing a Potentially Widespread Environmental Problem." *Environmental Pollution* 176: 114–22.

Megaw, P. 1999. The high-temperature, Ag-Pb-Zn-(Cu) carbonate replacement deposits of Central Mexico. In *VMS and carbonate-hosted Polymetallic deposits of Central Mexico.* Edited by J. L. Jambor. British Columbia and Yukon Chamber of Mines, Vancouver. pp. 25–44.

Mejía, J., Carrizales, L., Rodríguez, V.M., Jiménez-Capdeville, M.E., and Díaz-Barriga, F. 1999. Un método para la evaluación de riesgos para la salud en zonas mineras. *Salud Pública de México*, Vol. 41, pp. S132–S140. DOI: 10.1590/S0036-36341999000800010.

Mezned, N., Abdeljaouad, S., and Boussema, M.R. 2008. Caractérisation des rejets miniers dans le bassin versant de la Mejerda en utilisant les données ASTER. *Télédétection*, Vol. 8, No. 2, pp. 83–92.

Pinto-Linares, P. J., Levresse, G., Tritlla, J., Valencia, V. A., Torres-Aguilera, J. M., González, M., and Estrada, D. 2008. Transitional Adakite-like to calc-alkaline magmas in a Continental extensional setting at la PAZ Au-Cu Skarn deposits, mesa central, Mexico: metallogenic implications. *Revista Mexicana de Ciencias Geologicas*, Vol. 25, No. 1, pp. 39–58.

Pour, A.B., and Hashim, M. 2012. Identifying areas of high economic-potential copper mineralization using ASTER data in the Urumieh–Dokhtar volcanic belt, Iran. *Advances in Space Research*, Vol. 49, No. 4, 753–769. DOI: 10.1016/j.asr.2011.11.028.

Rajendran, S., Nasir, S., Kusky, T.M., Ghulam, A., Gabr, S., and El-Ghali, M.A.K. 2013. Detection of hydrothermal mineralized zones associated with Listwaenites in Central Oman using ASTER data. *Ore Geology Reviews*, Vol. 53, pp. 470–488.

Ramos-Arroyo, Y.R., and Siebe-Grabach, C.D. 2006. Estrategia para identificar jales con potencial de riesgo ambiental en un distrito minero: estudio de caso en el Distrito de Guanajuato, México. *Revista Mexicana de Ciencias Geologicas*, Vol. 23, No. 1, pp. 54–74.

Ramos-Arroyo, Y.R., Ledesma, R., and Grabach, C. 2004. Características geológicas y. mineralógicas e. historia de extracción del Distrito de Guanajuato, México. Posibles escenarios geoquímicos para los residuos mineros. *Revista Mexicana de Ciencias Geológicas*, Vol. 21, No. 2, pp. 268–284.

Razo, I., Carrizales, L., Castro, J., Díaz-Barriga, F., and Monroy, M. 2004. Arsenic and heavy metal pollution of Soil, water and sediments in a semi-Arid climate mining area in Mexico. *Water, Air, & Soil Pollution*, Vol. 152, No. 1-4, pp. 129–152. DOI: 10.1023/B:WATE.0000015350.14520.c1.

Rouskov, K., Popov, K., Stoykov, S., and Yamaguchi, Y. 2005. Some applications of the remote sensing in geology by using of ASTER images. In *Scientific Conference "Space, Ecology, Safety*." Varna, Bulgaria, *June 10-13*.

Rowan, L.C., Mars, J.C., and Simpson, C.J. 2005. Lithologic mapping of the Mordor, NT, Australia ultramafic complex by using the Advanced Spaceborne Thermal Emission and

Reflection Radiometer (ASTER). *Remote Sensing of Environment*, Vol. 99, No. 1-2, pp. 105–126. DOI: 10.1016/j.rse.2004.11.021.

Schimmer, R. 2008. A remote sensing and GIS method for detecting land surface areas covered by copper mill tailings. In *Pecora 17 - the future of land imaging...going operational*. *Denver, Colorado. November 18-20*.

SGM (Servicio geologico Mexicano) 2008. Minería. In *Monografía Geológico-Minera Del Estado de San Luis Potosí*, 273. Secretaria de economia, México. Available from [cited December 17, 2015].

Van Zyl, D., Sassoon, M., Digby, C., Fleury, M.A., and Kyeyune, S. 2002. *Mining for the future: main report*. IIED. (International Institute for Environment and Development). No. 68. Available from <http://pubs.iied.org/pdfs/G00560.pdf> [cited December 17, 2015].

Yamaguchi, Y., Fujisada, H., Kudoh, M., Kawakami, T., Tsu, H., Kahle, A.B., and Pniel, M. 1999. ASTER instrument characterization and operation scenario. *Advances in Space Research*, Vol. 23, No. 8, pp. 1415–1424. DOI: 10.1016/S0273-1177(99)00293-8.

Yáñez, L., García-Nieto, E., Rojas, E., Carrizales, L., Mejía, J., Calderón, J., Razo, I., and Díaz-Barriga, F. 2003. DNA damage in blood cells from children exposed to arsenic and lead in a mining area. *Environmental Research*, Vol. 93, No. 3, pp. 231–240. DOI: 10.1016/j.envres.2003.07.005.

Table 1. Band specifications and the spectral range of the ASTER system.

Subsystem	Band number	Spectral range (μm)	Spatial resolution (m)
VNIR	1	0.52 – 0.60	15
	2	0.63 – 0.69	
	3N	0.78 – 0.86	
	3B	0.78 – 0.86	
SWIR	4	1.600 – 1.700	30
	5	2.145 – 2.185	
	6	2.185 – 2.225	
	7	2.235 – 2.285	
	8	2.295 – 2.365	
	9	2.360 – 2.430	
TIR	10	8.125 – 8.475	90
	11	8.475 – 8.825	
	12	8.925 – 9.275	
	13	10.25 – 10.95	
	14	10.95 – 11.65	

Table 2. Band ratios used.

Feature	Band Ratio	Reference
Ferrous iron index in silicates and carbonates	B5/B4	Cudahy (2012) Rowan et al. (2005)
Silica index	B13/B10	Cudahy (2012)
Mg-OH group (calcite, dolomite, chlorite, epidote, amphibole, etc.)	(B6+B9)/(B7+B8)	

Table 3. Accuracy assessment results.

Classification	Classified data	Ground truth (pixels)			Accuracy (%)			
		a	b		Producer	User	Overall	*K*
Ferrous index	a	397	11		89.0	97.3	93.3	0.86
	b	49	432		97.5	89.8		
Silica index	a	34	6		100.0	85.0	91.2	0.82
	b	0	28		82.4	100.0		
Hematite 3	a	73	0		80.2	100.0	90.2	0.80
	b	18	92		100.0	83.6		
Quartz 2	a	329	5		73.8	98.5	86.3	0.72
	b	117	438		98.9	78.9		
Orthoclase 1	a	325	10		72.9	97.0	85.3	0.70
	b	121	433		97.7	78.2		
Mg-OH	a	85	32		100.0	72.7	81.1	0.62
	b	0	52		61.9	100.0		
NDTI	a	267	0		59.9	100.0	79.9	0.59
	b	179	443		100.0	71.2		

Confusion matrices of different classification were made, and the accuracy assessment results based on the evaluation sites are shown in Figure 1. a. Mine wastes; b. No mine wastes. NDTI represents the Normalized Difference Tailings Index.

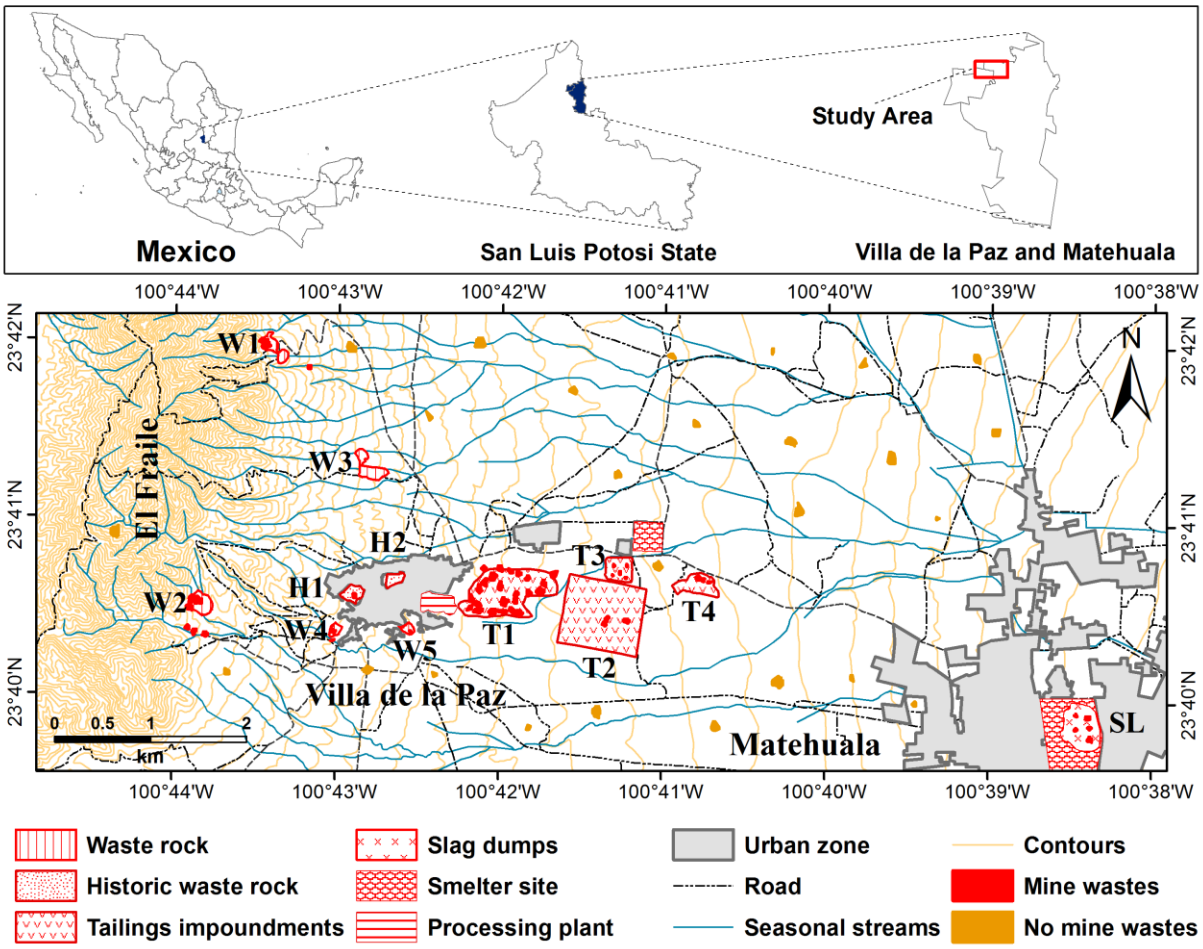

Figure 1. Geographical location and schematic description of the different types of mine wastes with the evaluation sites marked (red and orange points). The labels on this map are discussed in the text.

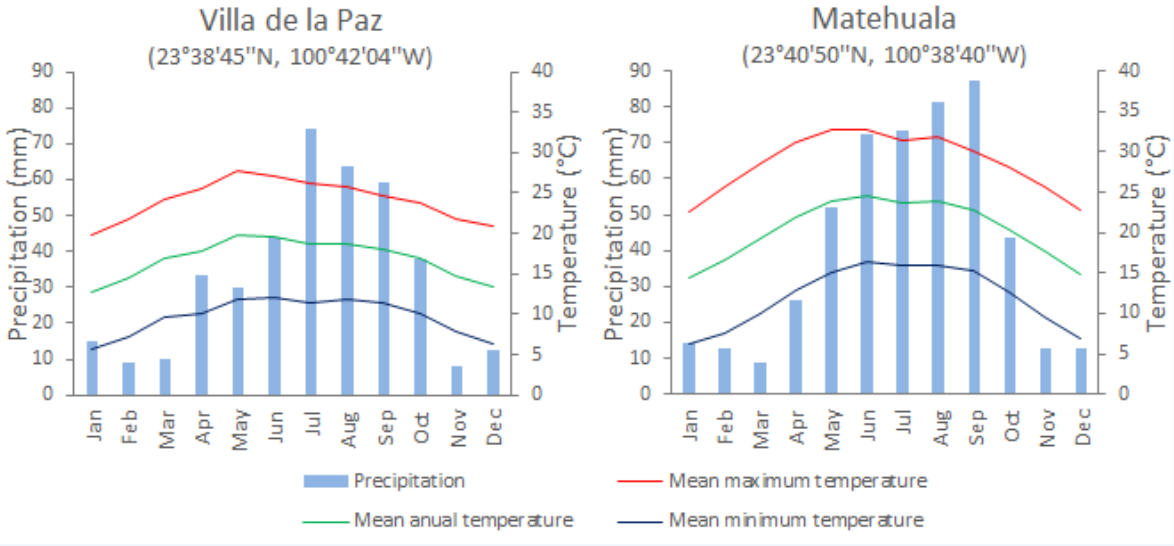

Figure 2. Climograms from meteorological stations in the study area.

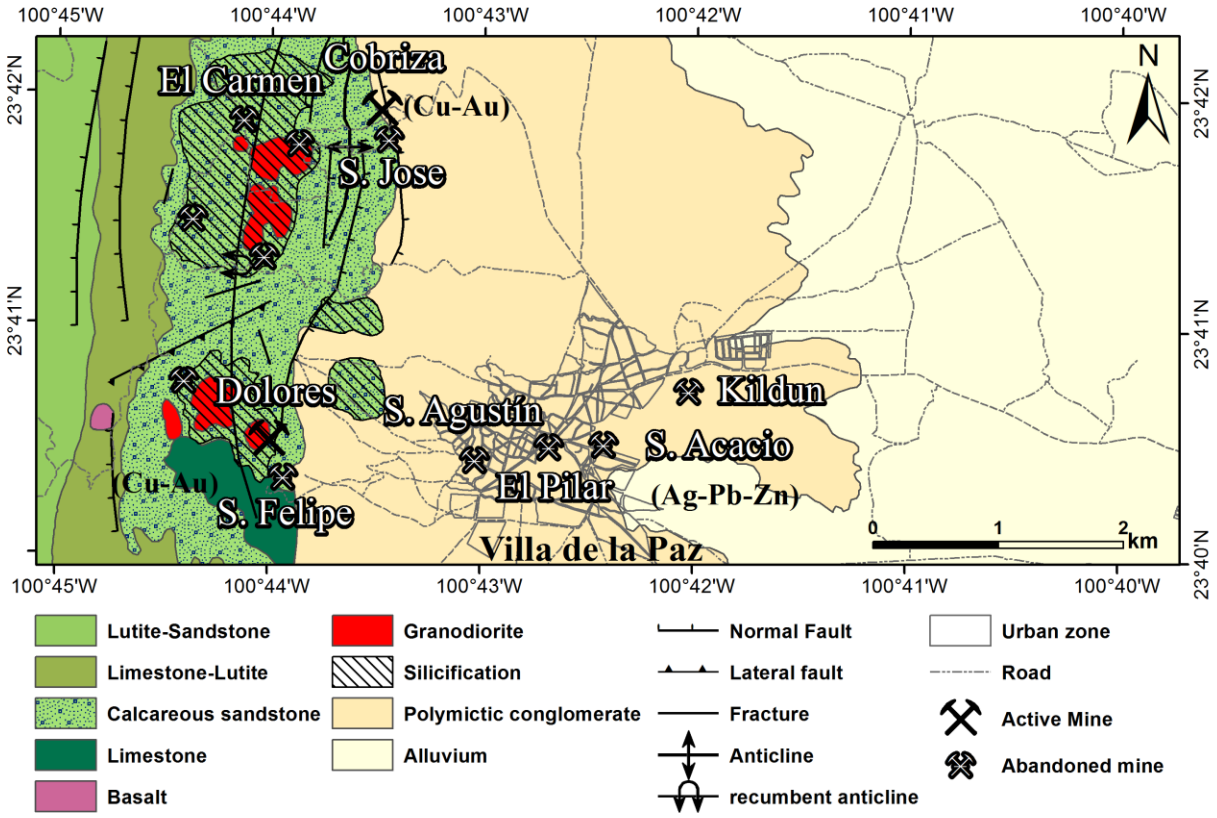

Figure 3. Geological features of the study area.

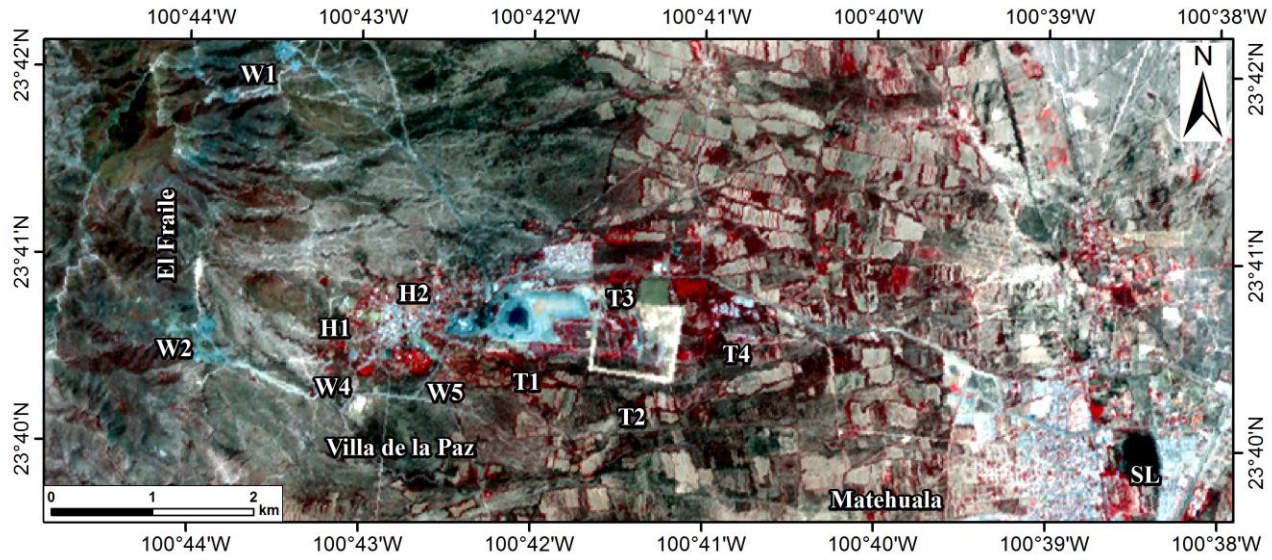

Figure 4 RGB 321 composite showing the subscene location of the original ASTER data used to classify the study area.

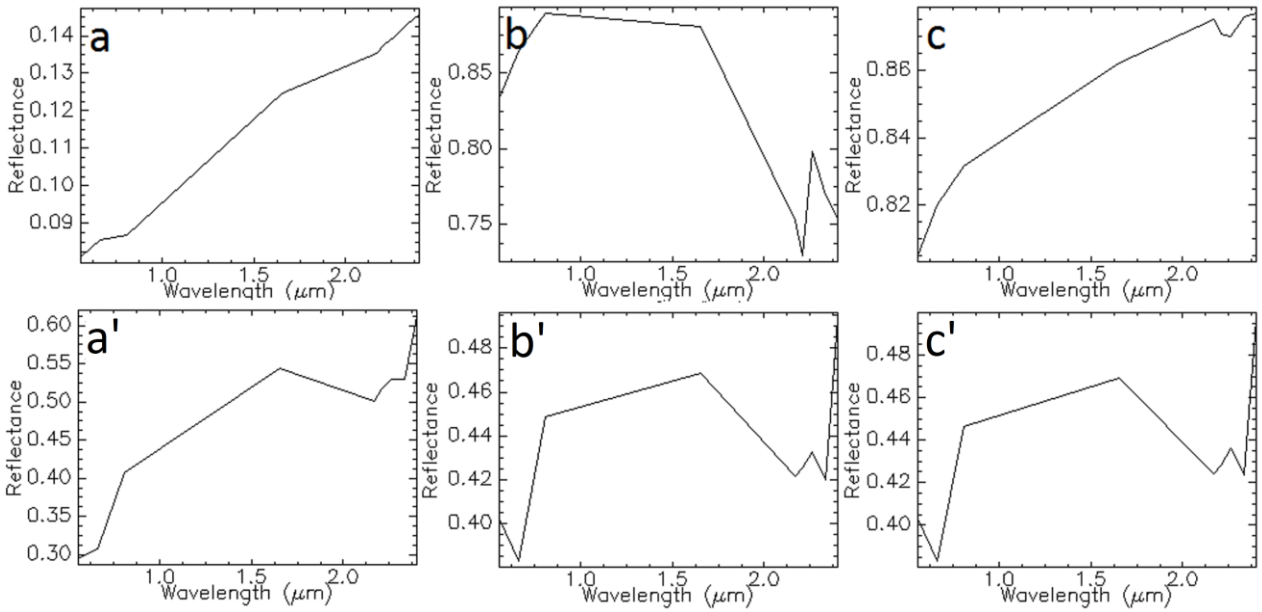

Figure 5. USGS reference spectra resampled to the ASTER spectral resolution for (a) hematite 3, (b) orthoclase 1, and (c) quartz 2. Also shown, pixel spectra derived from the SAM classification using a threshold of 0.08 radians for (a') hematite, (b') orthoclase and, (c') quartz.

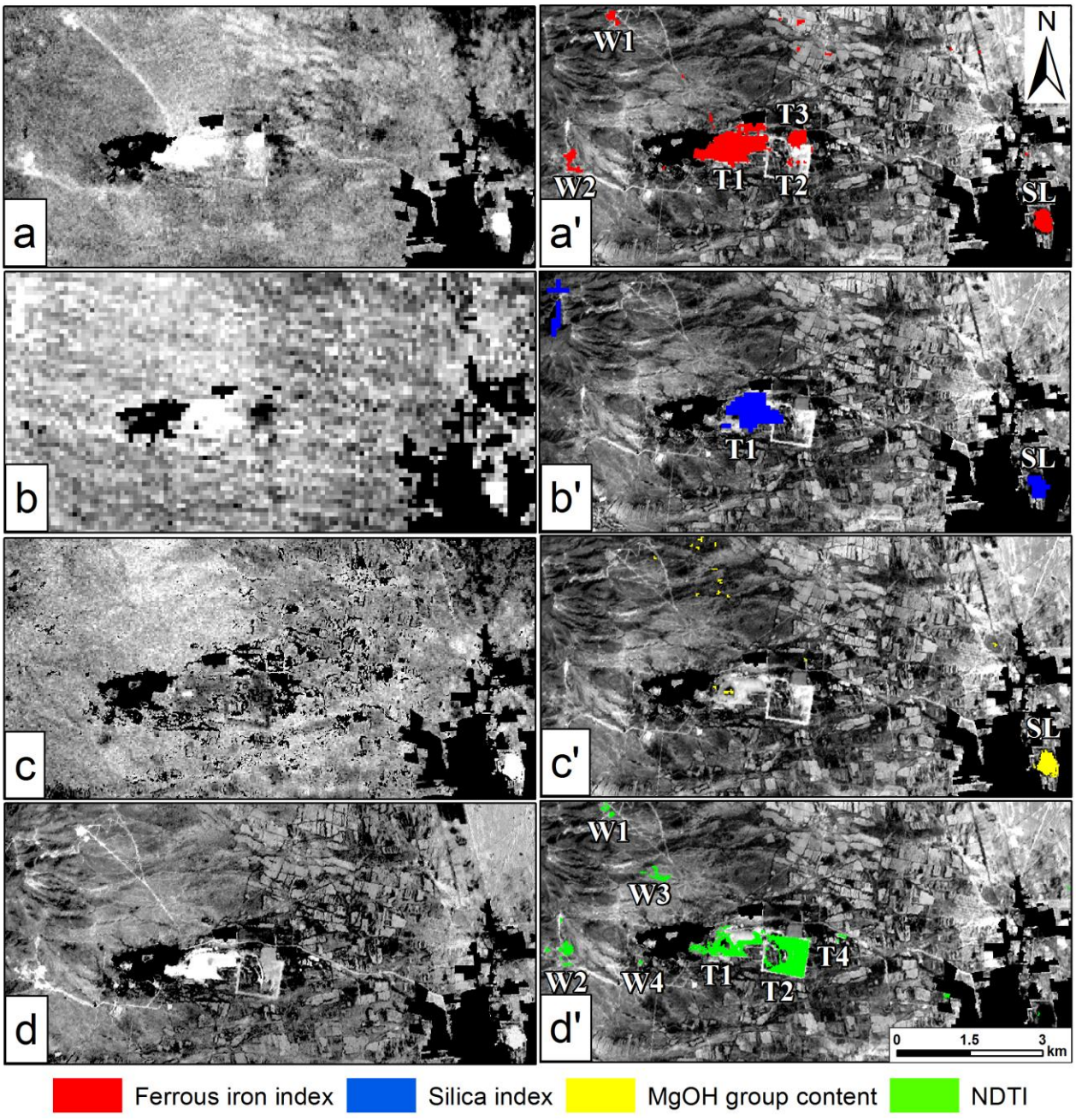

Figure 6. Output results for (a) ferrous iron index, (b) silica index, (c) Mg-OH group content and (d) NDTI operation. The segmentations are based on the mean value + 2.3 × the standard deviation, overlaid on band 2 of the ASTER scene.

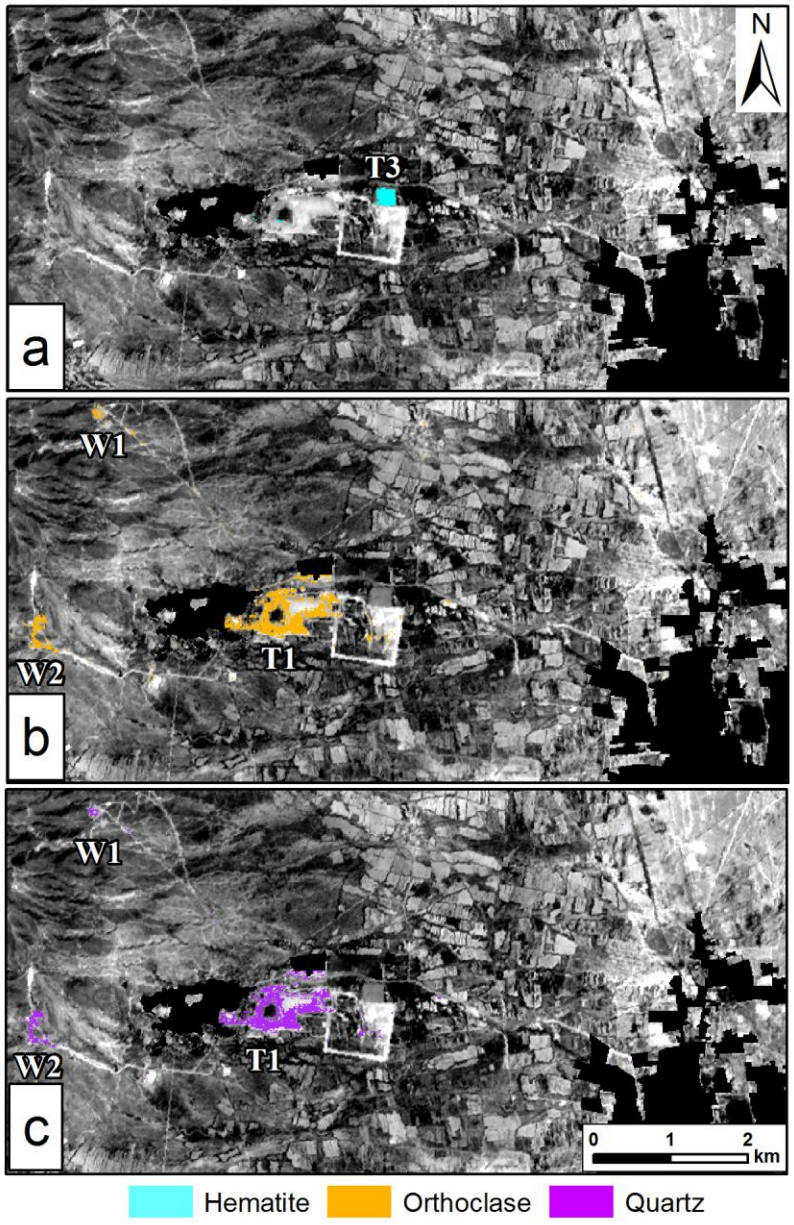

Figure 7. SAM classification results for (a) hematite, (b) orthoclase and (c) quartz, overlaid on band 2 of the 2006 ASTER scene.

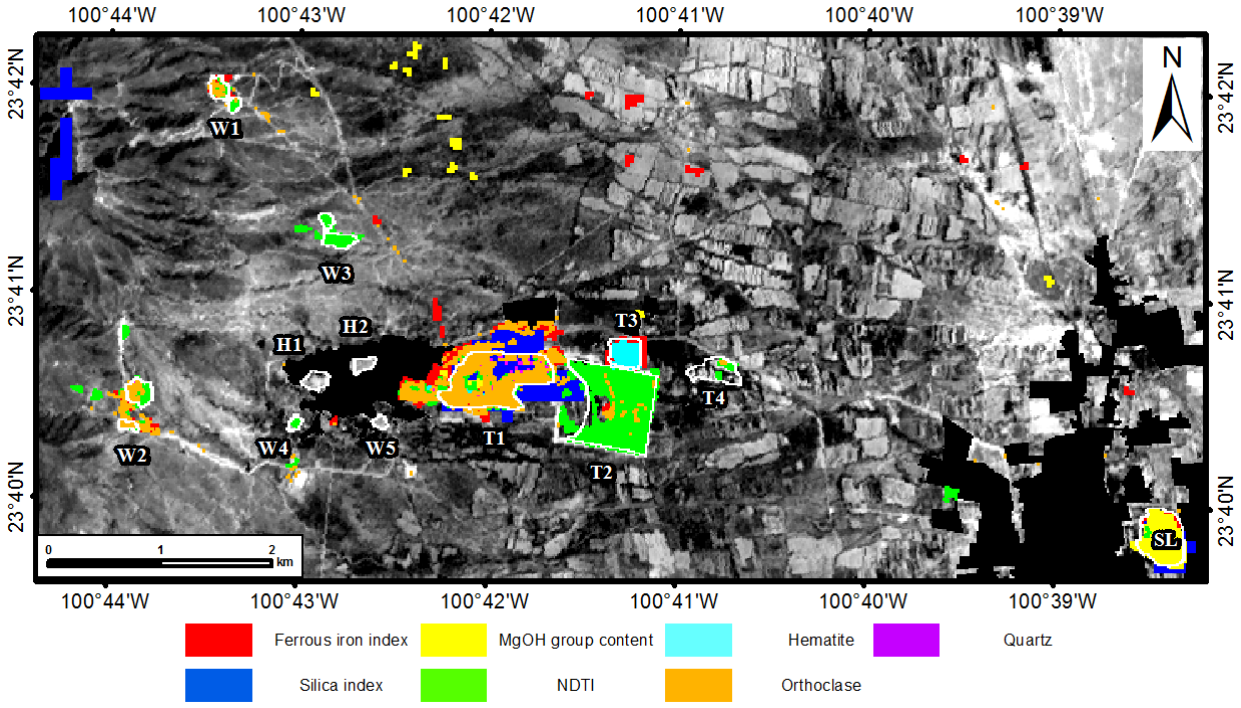

Figure 8 Final integration of the different classification results overlaid on band 2 of the ASTER scene. The known locations of the different mine wastes are enclosed by white polygons.